M-SrFe 12 O 19 and ferrihydrite-like ultrathin nanoplatelets as building blocks for permanent magnets: HAADF-STEM study and magnetic properties

Bilel Grindi, Amor Benali, Cesar Magén, G. Viau

M-$SrFe_{12}O_{19}$ and ferrihydrite-like ultrathin nanoplatelets as building blocks for permanent magnets: HAADF-STEM study and magnetic properties

Bilel Grindi,[a,b] Amor BenAli,[b,c] Cesar Magen,[d,e,f] Guillaume Viau[a,*]

[a]*Université de Toulouse, LPCNO, UMR 5215 INSA-CNRS-UPS, 135 av. de Rangueil 31077 Toulouse, France*

E-mail: gviau@insa-toulouse.fr

[b]*Synthèse et Structure des Nanomatériaux (UR11-ES30), Faculté des Sciences de Bizerte, Université de Carthage, 7021, Jarzouna, Tunisia*

[c]*Department of Chemistry, College of Science, Imam Abdulrahman bin Faisal University, Dammam, Saudi Arabia*

[d]*Instituto de Ciencia de Materiales de Aragón, Universidad de Zaragoza – CSIC, 50009 Zaragoza, Spain*

[e]*Departamento de Física de la Materia Condensada, Universidad de Zaragoza, 50009 Zaragoza, Spain*

[f]*Laboratorio de Microscopías Avanzadas (LMA), Instituto de Nanociencia de Aragon (INA), Universidad de Zaragoza, 50018 Zaragoza, Spain*

[*]corresponding author

E-mail address : gviau@insa-toulouse.fr

Abstract

Mixtures of *M*-type strontium hexaferrite (M-$SrFe_{12}O_{19}$) and ferrihydrite-like particles were prepared by a microwave-assisted hydrothermal process at 200 °C with heating rates in the range 40-50 °C.min^{-1}. The particles exhibited a platelet shape with a diameter comprised between 20 and 200 nm and a thickness between 2 and 5 nm. HAADF-STEM observations and EDS analysis were carried out for a better understanding of nucleation and growth process. EDS showed that most of the particles contained Sr and HAADF-STEM revealed that very thin particles with a hexaferrite core extending over less than a unit cell and with surface disorder crystallized along with well crystallized hexaferrite and defect free ferrihydrite particles. The symmetric multilayer structures (SRS) of the ultrathin particles suggested that the nucleation step of the hexaferrite particles involved clusters containing Sr atoms. In comparison with the M-$SrFe_{12}O_{19}$ micrometer sized platelets prepared with heating rate of 25 °C.min^{-1}, the mixtures of ultrathin hexaferrite- and ferrihydrite-like particles combined after annealing a higher coercivity reaching 465 kA.m^{-1} thanks to the smaller initial particle size and a high magnetization reaching 65 A.m^2.kg^{-1} thanks to a limited amount of hematite.

1. Introduction

Permanent magnets (PM) are essential in everyday life energy product ranging from large scale machines like high power wind mills to the smallest motors and actuators [1]. PM materials are dominated by two systems: the rare-earth based alloys (NdFeB and SmCo) and the barium and strontium hexaferrites. Despite they exhibit lower energy products than the rare-earth based magnets, the hexaferrite PMs are still used in lots of applications thanks to several advantages. They are produced at very low cost, they are chemically stable and not sensitive to oxidation, and they are based on non-critical elements. Powerful PMs based on hexaferrites require a good control of the particle size in the submicrometer range and alignment of the magnetic easy axis after compaction of the powders. Several elaboration processes were developed for the synthesis of hexaferrites, among them co-precipitation followed by an annealing at an optimum temperature [2]. M-$SrFe_{12}O_{19}$ powders with high coercivity were produced by hydrothermal synthesis at 130°C followed by calcination at 850 °C [3]. Several chemical parameters were varied to obtain pure $AFe_{12}O_{19}$ (A = Ba, Sr) phases by hydrothermal synthesis and to control the particle size [4,5,6]. The formation of pure phases is obtained in alkaline medium by controlling the M/Fe molar ratio in the starting mixtures. Large excess of barium or strontium in the starting mixtures is necessary to avoid the crystallization of hematite or other undesired phase as side product [4,5]. The heating temperature and reaction time allowed to control the particle size: ultrafine nanoparticles with a disk-like shape were obtained below 170 °C while larger platelets were formed at higher temperatures [6]. The influence of sodium hydroxide concentration on the phase formation was also studied [7] and microwave-assisted hydrothermal methods were used to prepare pure $BaFe_{12}O_{19}$ thin platelets within very short reaction time [8]. Other solvents like ethylene glycol/deionized water mixtures were also used at 200 °C [9]. M-$BaFe_{12}O_{19}$ nanorods were synthesized by the reaction of α-FeOOH nanorods and $BaCO_3$ at 220°C followed by a two-steps annealing [10]. Barium-doped iron oxide nanocubes were obtained by thermodecomposition process, using barium stearate as barium source, that can be converted easily to hexagonal barium ferrite [11]. In absence of surfactant or templating agent the hydrothermal syntheses in alkaline solution provide thin platelets with the crystallographic *c* axis perpendicular to the platelet.

Thin platelets are not generally considered as the best shape to get high coercivity because of the competition between the magnetocrystalline anisotropy and the demagnetizing effects but

present several advantages. Application of a magnetic field provokes the platelets orientation perpendicular to the applied field direction in agreement with a magnetocrystalline easy axis parallel the crystallographic *c* axis [12]. Furthermore, the self-assembly properties of platelets were also exploited in different studies. $BaFe_{12}O_{19}$ thin platelets were used as building blocks to form oriented films with highly anisotropic magnetic behavior by electrophoretic deposition [13]. Ferrofluids with very small $BaFe_{12}O_{19}$ platelets were obtained using oleic acid as stabilizing agent [14] and field dependent optical properties were described on colloidal solutions of $SrFe_{12}O_{19}$ plate-like nanoparticles [15]. Nanometre-sized $BaFe_{11.5}Sc_{0.5}O_{19}$ ferromagnetic platelets synthesized by hydrothermal method and suspended in a nematic liquid crystal can constitute a new class of multiferroic materials [16]. Saura-Múzquiz et *al.* showed recently that compaction of hexaferrite platelets by Spark Plasma Sintering could give materials with a very high degree of alignment, even in absence of any applied magnetic field, and consequently provide high energy products [17]. Another interest of the nanoplatelets prepared by the hydrothermal methods is the possibility to grow another oxide at their surface to make "sandwich" platelets. Primc et al. exploited this opportunity to combine hard and soft magnetic materials in the same platelet [18].

Despite hexaferrite particles synthesis by hydrothermal methods is now well established, only few studies reported on the growth mechanism and thorough structural characterization of the solid intermediate phases before the high temperature annealing step. Based on X-ray diffraction patterns it was suggested that mixtures of goethite α-FeO(OH), hematite α-Fe_2O_3, hexaferrite $SrFe_{12}O_{19}$ and $SrFeO_{2.5}$ could be intermediate phases of $SrFe_{12}O_{19}$ powders by hydrothermal synthesis [3]. Ultrathin $BaFe_{12}O_{19}$ nanoparticles prepared at lower temperature (150 °C) were analyzed using high resolution microscopy, X-ray absorption and Mössbauer spectroscopy by Makovec *et al.* [19]. The authors concluded that the particles crystallized with a strongly disordered hexaferrite structure. Granados-Miralles *et al.* described the synthesis of pure hexaferrite particles with ferrihydrite as intermediate phase [20]. The formation of pure hexaferrite at high temperature was obtained after a ripening process that involved the progressive dissolution of the ferrihydrite particles [20]. Interestingly, ultrathin hexaferrite platelets may exhibit composition and structure differing from bulk hexaferrite. $BaFe_{12}O_{19}$ and $SrFe_{12}O_{19}$ crystallize in the magnetoplumbite hexagonal structure (space group $P6_3/mmc$) that can be described as alternating stacking along the *c*-axis of R and S blocks, respectively

$(AFe_6O_{11})^{2-}$ (A = Ba, Sr) and $(Fe_6O_8)^{2+}$. The unit cell can be described as the RSR^*S^* stacking sequence along the *c*-direction, where the asterisk denotes the screw axis symmetry 6_3 along *c*. Recently, B. Belec *et al.* isolated very thin nanoplatelets limited to the stacking sequence SR^*S^*RS paving the way to a chemical engineering of new layered nanostructures [21].

In this work, platelet shaped strontium-iron oxides were synthesized by a microwave-assisted hydrothermal method at 200°C and characterized by scanning transmission electron microscopy coupled with high angle annular dark field imaging (HAADF-STEM) performed on a probe corrected electron microscope equipped with a cold field emission gun. The microwave heating rate has a strong influence on the particle morphology and structure. The very small platelets prepared with the highest heating rates particles are the best precursors for high coercivity after annealing at 1000 °C. A special attention has been given to HAADF-STEM characterization of these ultrathin platelets for a better description of the nucleation/growth mechanism. An original SRS stacking is reported.

2. Experimental

2.1. Synthesis

Iron (III) nitrate nonahydrate $Fe(NO_3)_3.9H_2O$ (Strem Chemicals) and strontium nitrate $Sr(NO_3)_3$ (Alfa Aesar) were dissolved in demineralized water in various ratios. The obtained solution was afterwards added drop by drop, under argon atmosphere, in an aqueous sodium hydroxide NaOH (Sigma-Aldrich) solution. In all experiments, iron (III) concentration in the solution after mixing was fixed at 0.8 M, the molar ratio Fe/Sr at 3 and the pH of the starting mixture at 10.

These solutions were subsequently transferred in a Teflon beaker EasyPrep reactor and heated at 200 °C for one hour in a microwave oven CEM Mars 6 (2.45 GHz, maximum power 650 W). The heating rate was varied between 10 and 50 °C.min^{-1}.

After 1h heating at 200 °C the precipitate was cooled to room temperature, centrifuged, washed several times with diluted solution of acetic acid (0.1 M), demineralized water and ethanol. The resulting powder was dried at 50°C for 12 hours. The first washing with the diluted acetic acid solution aims to remove the undesired Sr-rich phases that precipitate with the $SrFe_{12}O_{19}$ due to the excess of strontium in the starting mixture. These particles were characterized by X-ray diffraction, electron microscopy, energy dispersive spectroscopy and magnetometry. The powders were annealed in air at 1000 °C and then characterized by X-ray diffraction, electron

microscopy and magnetometry.

2.2. Characterizations

X-ray diffraction (XRD) pattern were recorded on a PANalytical Empyrean diffractometer in the 2θ range 10-90°, using CoKα radiation (λ= 1.789/1.792Å). The unit cell parameters were refined by full pattern matching simulation [22] with the FULLPROF program [23]. The raw particles morphology was studied by transmission electron microscope (TEM) at 100 kV with JEOL JEM1011 microscope. The particles were dispersed in ethanol and sonicated, one drop of the suspension was deposited on a carbon coated copper grid and the solvent was evaporated at room temperature under vacuum. Scanning transmission electron microscopy coupled with high angle annular dark field imaging (HAADF-STEM) observations were performed on a probe corrected JEOL JEM-ARM200F instrument equipped with a cold field emission gun. HAADF-STEM image simulations of thin platelets with thickness in the range 4-8 nm have been carried out using the multislice method with the QSTEM software package [24]. Annealed powders were observed by field emission gun scanning electron microscopy (FEG-SEM) using a JEOL JSM7800F microscope. Magnetic measurements were carried out using Quantum Design Physical Property Measurement System (PPMS) in Vibrating Sample Magnetometer (VSM) configuration. Magnetization loops, M(H), were recorded at 300K with applied field varying between ± 5T. The highest field value was generally not enough to reach the magnetization saturation of the powders. The saturation magnetization values, Ms, were determined by extrapolating the M(1/H) curves to 1/H = 0.

3. Results and Discussion

3.1. Microwave synthesis and annealing

Several powders were prepared by heating aqueous solutions of iron and strontium nitrate in for 1 h at 200 °C using a microwave oven. The heating rate (HR) was varied between 10 and 50 °C.min^{-1} while the other parameters like the Fe/Sr ratio and the pH of the solutions were fixed in all experiments (see experimental details). Transmission electron microscope (TEM) observations on powders prepared with different heating rates (HRs) showed platelet-like nanoparticles with a mean diameter that decreased when the HR was increased (Figure 1). Thin platelets with a micrometric diameter were obtained for HR up to 27 °C.min^{-1} (Figure 1a). The mean diameter decreased to 25 nm with an HR of 49 °C.min^{-1} (Figure 1d) and for intermediate

HRs a broad diameter distribution was generally observed (Figure 2b,c). The thickness of the small platelets prepared with high HR was measured on dark field images and was found in the range of 2-5 nm (Figure 1e).

The powder X-ray diffraction (XRD) patterns were found to strongly depend on HR (Figure 2). For the lower HRs the XRD patterns exhibit the strong lines of M-$SrFe_{12}O_{19}$ hexaferrite and weak lines of hematite (α-Fe_2O_3) (Figure 2a,b). Hematite weight fraction estimated by Rietveld analysis was 6 and 2 %, for HRs of 12 and 20 °C.min^{-1}, respectively. The hematite peaks were no more present for HR = 27 °C.min^{-1} and the XRD pattern could be indexed as pure M-$SrFe_{12}O_{19}$ phase (Figure 2c). For higher HR the intensity of the M-$SrFe_{12}O_{19}$ peaks progressively decreased and seven broad lines at the distances 2.538 Å, 2.447 Å, 2.227 Å, 1.963 Å, 1.710 Å, 1.497 Å and 1.465 Å appeared (Figure 2d,e). These seven lines fit well with the XRD pattern of ferrihydrite reported by Berquó *et al.* [25]. The ferrihydrite is a Fe(III) oxyhydroxide that crystallizes as a mixture of a defect free phase (f-phase) and a defective phase (d-phase) with small amount of hematite in variable proportion [26,27,28]. Both f- and d-phases present a hexagonal structure with parameters a = 2.955 Å and c = 9.370 Å but differs from the space groups, P-31c for the f-phase and P3 for the d-phase [27]. The f-phase consists in a ABACA anionic packing in which the Fe atoms occupy the octahedral sites. The d-phase has a structure similar to the feroxyhite, δ-FeOOH, it is modelled as random sequences of ABA and ACA anionic layers with high degree of cation ordering [29]. Unit cells of f-phase and d-phase are given as supplementary information along with the strontium hexaferrite and hematite unit cells (Figure S1-S4). XRD pattern of ferrihydrite synthesized at low temperature generally exhibits six lines but a seventh one can be observed in case of good crystallinity [25,30]. The peak positions measured experimentally on the pattern of Figures 2d-e are consistent with (100), (101), (102), (103), (104), (105) and (110) reflexions of a hexagonal phase with parameters a = 2.93 Å and c = 9.27 Å, thus very close to the ferrihydrite parameters. For the highest heating rate (Figure 2e), the broad hexaferrite lines are almost totally screened by the ferrihydrite bands.

The saturation magnetizations (M_S) of the grown powders prepared with different HR are reported in Table 1. The highest value, M_S = 63 emu.g^{-1}, was obtained for the pure M-$SrFe_{12}O_{19}$ phase prepared with HR = 27 °C.min^{-1}. For HR = 12 °C.min^{-1} a lower M_S value is explained by the presence of small amount of hematite that exhibits a magnetization close to zero. The very small M_S values obtained with the highest HRs is related either to a large amount of ferrihydrite,

which is antiferromagnetic at room temperature [27], and/or to an important amount of ultrathin hexaferrite particles as was described before by Primc *et al.* [6].

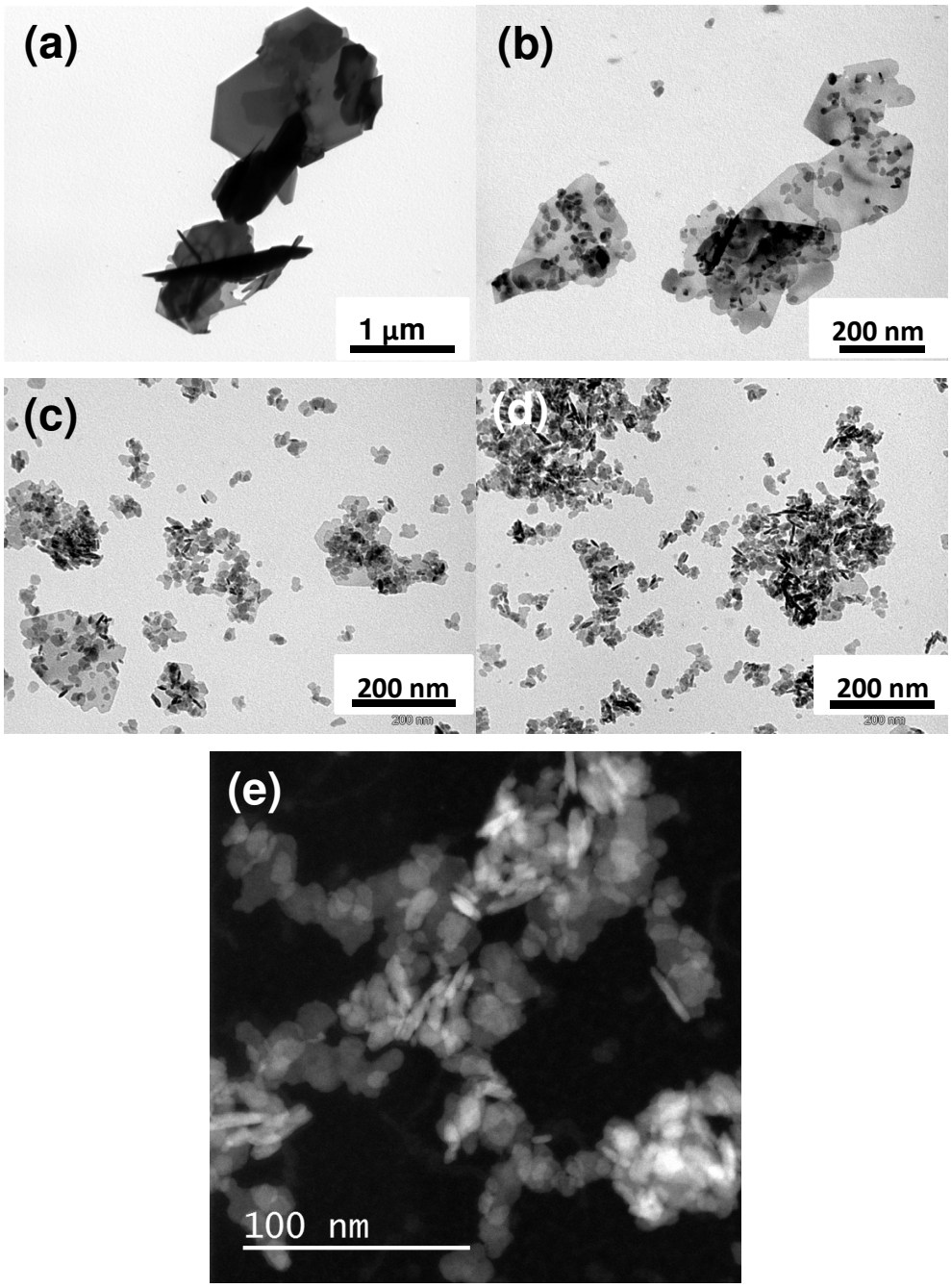

Fig. 1. TEM images of powders obtained with different heating rate, (a) 27 °C.min^{-1}; (b) 35 °C.min^{-1}; (c) 41 °C.min^{-1} and (d) 49 °C.min^{-1}; (e) HAADF-STEM images of particles prepared with a heating rate of 49 °C.min^{-1}.

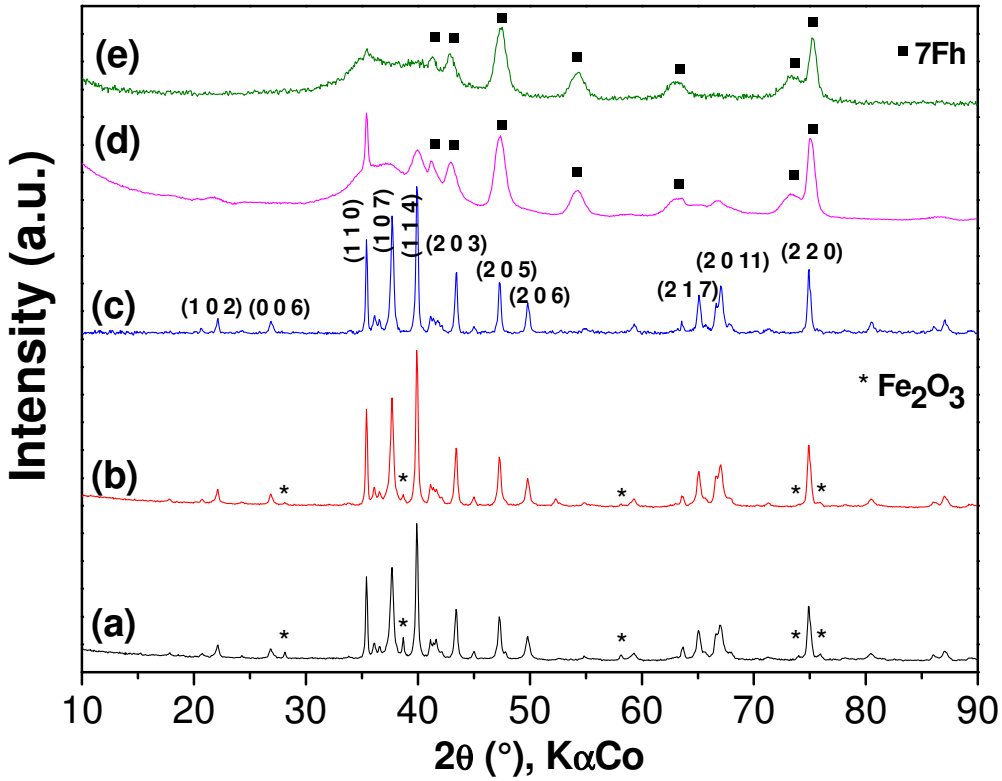

Fig. 2. XRD patterns of powders obtained with different heating rate, (a) 12 °C.min^{-1} ; (b) 20 °C.min^{-1} ; (c) 27 °C.min^{-1} ; (d) 41 °C.min^{-1} ; (e) 49 °C.min^{-1}. The asterisk symbols (*) denote the main peaks of hematite (α-Fe_2O_3), the black squares denote the main peaks of seven line ferrihydrite (7Fh).

After annealing the XRD patterns were identified as mixtures of M-$SrFe_{12}O_{19}$ and hematite (Figure S5). The weight fractions of hematite $x_{Fe_2O_3}$ determined by Rietveld analysis are reported in Table 1. $x_{Fe_2O_3}$ is significantly higher when a mixture of ferrihydrite and strontium hexaferrite was obtained with the highest HRs, but never exceeded 16 % (Table 1). The saturation magnetization, M_S, of the powders after annealing is very well fitted by the relationship Ms(A.m^2.kg^{-1}) = 75.5×(1-$x_{Fe_2O_3}$) (Figure 3) showing that the saturation magnetization of the annealed powders is proportional to the weight fraction of M-$SrFe_{12}O_{19}$ as expected for mixtures of a ferromagnetic (strontium hexaferrite) and an antiferromagnetic phase (hematite). The saturation magnetization M_S = 75.5 A.m^2.kg^{-1} is in very good agreement with Ms value reported

in the literature for M-$SrFe_{12}O_{19}$ [31]. Annealing of the almost pure strontium hexaferrite powders with the lowest HR involved mainly a crystallinity improvement [32] while annealing of the powders prepared with high HR caused the disappearance of the ferrihydrite phase and the crystallization of the strontium hexaferrite along with hematite in small amount. The phase transformation of ferrihydrite into hematite at high temperature is well documented [33,34]. The limited content of hematite after annealing in the samples prepared with HR = 41 and 49 °C.min^{-1} can be interpreted either by a limited content of ferriydrite in the raw samples and/or by the reaction of ferrihydrite particles with Sr-rich particles giving additional hexaferrite particles. More details on the particle local composition inferred from electron micrsocopy are given in the next section.

The coercivity of the magnetization loops, H_C, increased after annealing (Table 1) in agreement with the crystallization of M-$SrFe_{12}O_{19}$ which is a hard magnetic material. It is noteworthy that the highest values, H_C = 455 – 465 kA.m^{-1}, were obtained with the powders generated from the smallest particles, i.e. from the particles prepared with the highest HRs (Figure 4). The particle shape modification with annealing was examined by SEM (supplementary information, Figure S6). For the samples prepared with low HR the platelet shape with high aspect ratio was retained after annealing (Figure S6a-b). On the contrary, the nanometre size platelets obtained with the highest HRs transformed after annealing into isotropic particles with a mean size in the sub-micrometre range (Figure S6c-d). The smaller mean crystallite size and their rounded shape can explain the higher coercivity. Indeed, above a critical size the magnetic particles adopt multi-domain configurations making easier the magnetization reversal. Moreover, the magnetocrystalline easy axis of the hexaferrite is the *c* axis. For very thin and large platelets, the magnetocrystalline anisotropy tends to align the magnetization along *c* while the demagnetizing effect tends to align the magnetization in plane. This competition makes easier the magnetization reversal, explaining the lower coercivity values of the large platelets.

Table 1. Synthesis conditions, mean diameter (D_m) and magnetic properties of particles prepared by microwave synthesis using different heating rates before annealing ; weight fraction of hematite and magnetic properties after annealing for 1 h at 1000 °C.

Microwave heating rate (°C.min^{-1})	Before annealing			After annealing 1000 °C		
	D_m (nm)	M_S (A.m^2.kg^{-1})	H_C (kA.m^{-1})	$x_{Fe_2O_3}$ (% wt.)	M_S (A.m^2.kg^{-1})	H_C (kA.m^{-1})
12	1700	56	102	0.25	75	315
27	1000	63	95	0	77	362
35	25-500	39	150	4.3	73	398
37	20-400	19	120	13.6	65	398
41	18-100	13	100	13.8	64	465
49	21-50	6	45	15.3	62	454

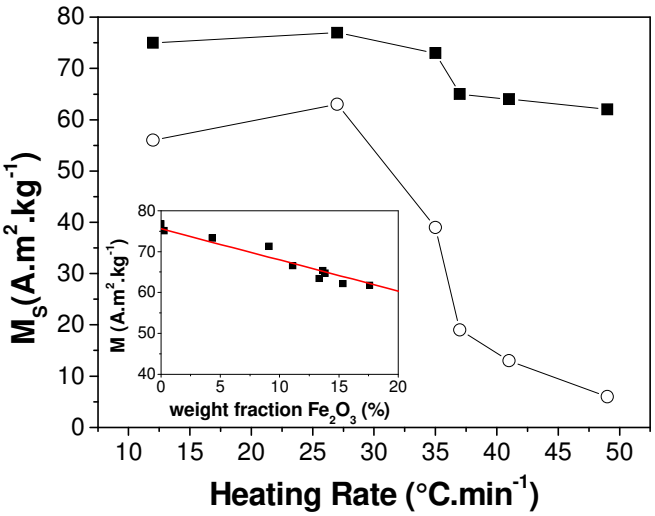

Fig. 3. Saturation magnetization of the powders synthesized with different heating rates before (○) and after annealing at 1000 °C for 1h (■). *Inset*: Saturation magnetization values vs weight fraction of hematite in annealed powders.

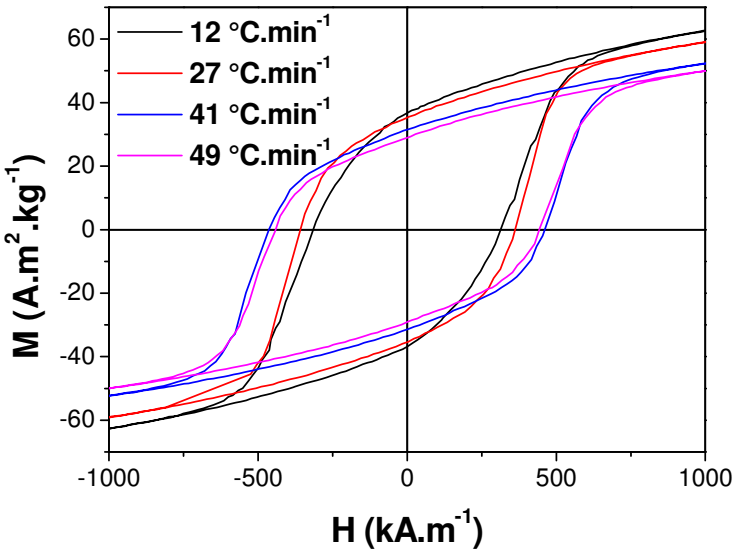

Fig. 4. Magnetization curves of powders obtained with different heating rate and annealed at 1000 °C.

3.2. HAADF-STEM study of ferrihydrite and strontium hexaferrite particles

In order to have a deeper insight into the very small particles prepared with the highest HRs, local EDS analysis and HAADF-STEM imaging were carried out. Strontium was detected in most of the particles but local inhomogeneity on the chemical composition was observed. Only very few particles did not contain any strontium which seems contradictory with the XRD pattern showing ferrihydrite as main component. On large areas and also on several isolated particles the Fe/Sr ratio was found very close to 12, i.e. the stoichiometric ratio of the M-$SrFe_{12}O_{19}$ phase. At a more local scale the atomic ratio Fe/Sr varied in the range 7-20 (more details are given in the supplementary information, Figures S7-S12).

HAADF-STEM images of representative particles prepared with HR of 41 or 49 °C.min^{-1} are given in Figures 5-8 and as supplementary materials (supplementary information). Several platelets were identified as strontium hexaferrite in [0001] zone axis like the one showed on Figure 5(a). The fast Fourier transform (FFT) of the HAADF image exhibits six spots indexed as the $\{11\bar{2}0\}$ reflections and six spots indexed as the $\{20\bar{2}0\}$ reflections (Figure 5b). The $\{10\bar{1}0\}$

reflections could not be detected on the diffraction pattern, in agreement with the M-$SrFe_{12}O_{19}$ structural model for which the relative intensity $I_{(10\bar{1}0)}$ is only 2 % of $I_{(11\bar{2}0)}$ [35]. The parameter a = 5.75 Å deduced from the calculated diffraction pattern is slightly smaller than the cell parameter of the reference pattern a = 5.8836 Å [35]. The Fourier filtered HAADF image (Figure 5c) is very similar to the simulated image of a 4 nm thick M-$SrFe_{12}O_{19}$ platelet (Figure 5d). The intensity recorded along the $[10\bar{1}0]$* direction presents the expected periodicity over 5 atomic columns (Figure 5e). In a rough approximation based on Rutherford scattering, HAADF-STEM image contrast of thin samples is proportional to the thickness and to Z^2 (Z being the atomic number). The power law observed experimentally is generally Z^{α} with α slightly lower than 2. Thus, as the oxygen atomic number is much lower than those of the metal atoms, the oxygen atom contribution to the HAADF images can be neglected. In the [0001] zone axis the columns observed along the $[10\bar{1}0]$* direction contain successively 1 Sr + 4 Fe, 2 Fe, 4 Fe, 2 Fe, 1 Sr + 4 Fe atoms (Figure 5f-g and Figure S1 given in supplementary information). Considering that the M-$SrFe_{12}O_{19}$ platelet thickness is constant the relative intensities estimated in the Z^2 approximation are thus 100 % - 32.6 % - 65.2% - 32.6% - 100 %. The intensities scattered by the atomic columns between the points A and B follow the same sequence (Figure 5e) showing a good agreement between the experimental image and this estimation.

Besides the strontium hexaferrite particles a large number of platelets exhibited a diffraction pattern of a hexagonal structure in [0001] zone axis with a parameter a = 5.85 Å i.e. very close to the lattice parameter of M-$SrFe_{12}O_{19}$ (Figure 6). Nevertheless the main difference with the diffraction pattern of the strontium hexaferrite particles was the presence of six spots indexed as the $\{10\bar{1}0\}$ reflexions (Figure 6b) revealing an atomic pattern different from strontium hexaferrite. As a matter of fact, the filtered dark field images of different areas of the platelet showed strong local variations on the cation sub-lattice (Figure 6c-d). The crystallographic coherence of the atomic pattern was generally limited to 5 nm (Figure 6d). It is noteworthy that despite such a cation occupation disorder, the diffraction pattern of the platelet is typical of a single crystal particle which can be explained by a very good order of the anion sub-lattice.

Few platelets were oriented edgewise providing useful information on the atomic stacking along the c axis. The stacking of metal atom layers is clearly evidenced on the HAADF-STEM image

of the 2.5 nm thick platelet presented on Figure 7. The Sr content measured by EDS in the central part of the platelet was found higher than the stoichiometry (Figure 7b). The very bright contrast of the central layer in the HAADF-STEM image is also in agreement with a Sr-rich atomic layer (Figure 7a). The contrast on the filtered image and the interlayer distances (Figure 7c) permitted to identify seven metal atom layers corresponding to the following stacking sequence along the *c* axis of the M-type strontium hexaferrite structure: Fe(5)/ Fe(3)-Fe(1)-Fe(3)/ Fe(5)/ Fe(4)-Sr+Fe(2)-Fe(4)/ Fe(5)/ Fe(3)-Fe(1)-Fe(3)/ Fe(5) (see more details on the Fe atoms labelling in the hexaferrite structure in supplementary information, Fig. S1). This stacking can be described as a SRS stacking of M-$SrFe_{12}O_{19}$ structure in $[10\bar{1}0]^*$ zone axis (Figure 7d). On this stacking additional outer layers have grown with disorder. This finding may explain the differences on the HAADF images of sidewise platelets. A well crystallized core with a reduced extent along *c* and showing disorder in the surface shells could exhibit a contrast variation on the HAADF images like the one of Figure 6. On the contrary, the atomic pattern of Figure 5 requires well crystallized and thick enough platelets with hexaferrite structure. Another example of SRS stacking with surface disorder is given in supplementary information (Fig. S9).

A few particles did not contain any strontium and were identified as ferrihydrite particles. On Figure 8 is given an example of such a platelet viewed sidewise. The calculated FFT pattern can be indexed as the diffraction pattern of a hexagonal phase in [0001] zone axis with parameter *a* = 2.9 Å (Fig. 8b). This value is very close to the lattice parameter value of both the defect free and the defective ferrihydrite, *a* = 2.9550 Å [26,27,28]. The Fourier filtered image revealed a pattern with two cation columns by unit cell (Fig. 8c). The ABACA anionic packing in the defect free ferrihydrite gives the possibility to the Fe atoms to occupy two different columns (Fig. 8f,g) contrary to the defective ferrihydrite that exhibit only one Fe column per unit cell (see Figs. S2-3 in supplementary information). The intensity scattered by the atomic columns is not constant (Fig. 8e) showing a disorder on the metal atom occupancy in agreement with the structural model that was proposed from XRD and neutron diffraction. This metal atom pattern is similar to the simulated HAADF image of the defect free ferrihydrite deduced from this model (Fig. 9d). It is noteworthy that the simulated HAADF image exhibits more disorder than the experimental one. One reason may be the rather good crystallinity of the ferrihydrite phase in comparison with the model that was proposed for 6 lines ferrihydrite powders elaborated at lower temperature and

that includes the disorder on the metal atom occupancy [26,27]. This also may confirm the seven lines of the experimental XRD pattern that are a feature of good crystallinity. Another defect free ferrihydrite platelet viewed edgewise is also given as supplementary materials (Figure S11). Very few particles that did not contain strontium exhibited a diffraction pattern very similar to the defect free ferrihydrite particles in the (0001) zone axis but with a different atomic pattern (see supplementary information Figure S12). These particles were identified as defective ferrihydrite in the (0001) zone axis with the cell parameter a = 2.9 Å and an atomic pattern that contains a single Fe atom column per unit cell (Figure S11). However a hematite particle in (111) zone axis cannot be discarded since the projections of the Fe sub lattices of defective ferrihydrite in (0001) zone axis and of hematite in (111) zone axis are exactly the same (Figure S12).

Finally, EDS analysis showed also platelets exhibiting Sr content higher than the hexaferrite stoichiometry. On figure S12 (see supplementary information) is given an example of a platelet with atomic ratio Fe/Sr = 7. The fast Fourier transform (FFT) of the HAADF image showed a diffraction pattern similar to the hexaferrite one but a closer examination revealed an orthorhombic distortion (Fig. S12b). The atomic pattern on Fourier filtered HAADF image (Fig. S12c) also differed from the hexaferrite pattern (Fig. 5c). Intensity plotted along three pseudo $[10\bar{1}0]$* directions revealed an intensity profile very different from the hexaferrite pattern for one direction while for the two others profiles were similar to the profile measured on the hexaferrite HAADF images with a periodicity over five atomic columns (Fig. S12c), in agreement with an orthorhombic distortion.

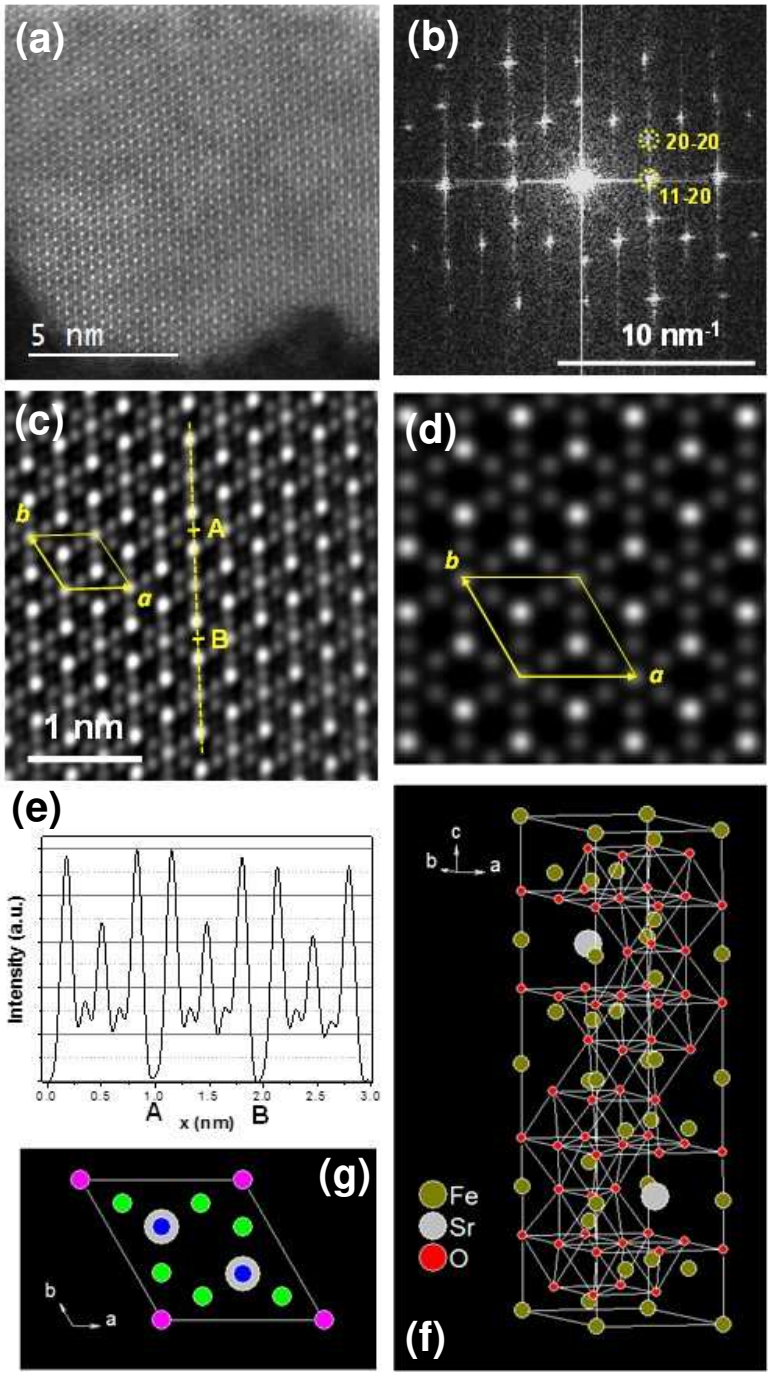

Fig. 5. (a) HAADF-STEM image of an hexaferrite nanoparticle; (b) Calculated FFT of the central part of the image indexed as a hexagonal phase in [0001] zone axis with quasi extinction of the $\{10\bar{1}0\}$ reflections; (c) Zoom on the Fourier filtered image; (d) HAADF-STEM image simulation of a 4 nm thick $SrFe_{12}O_{19}$ platelet in [0001] zone axis; (e) Intensity profile along the $[01\bar{1}0]^*$ direction (dashed line on filtered image); (f) unit cell of the $SrFe_{12}O_{19}$ hexaferrite; (g) projection of the cationic columns in [0001] zone axis showing the three different kind of columns per unit cell, blue+grey = 4Fe +1Sr, magenta = 4 Fe, green = 2 Fe atoms.

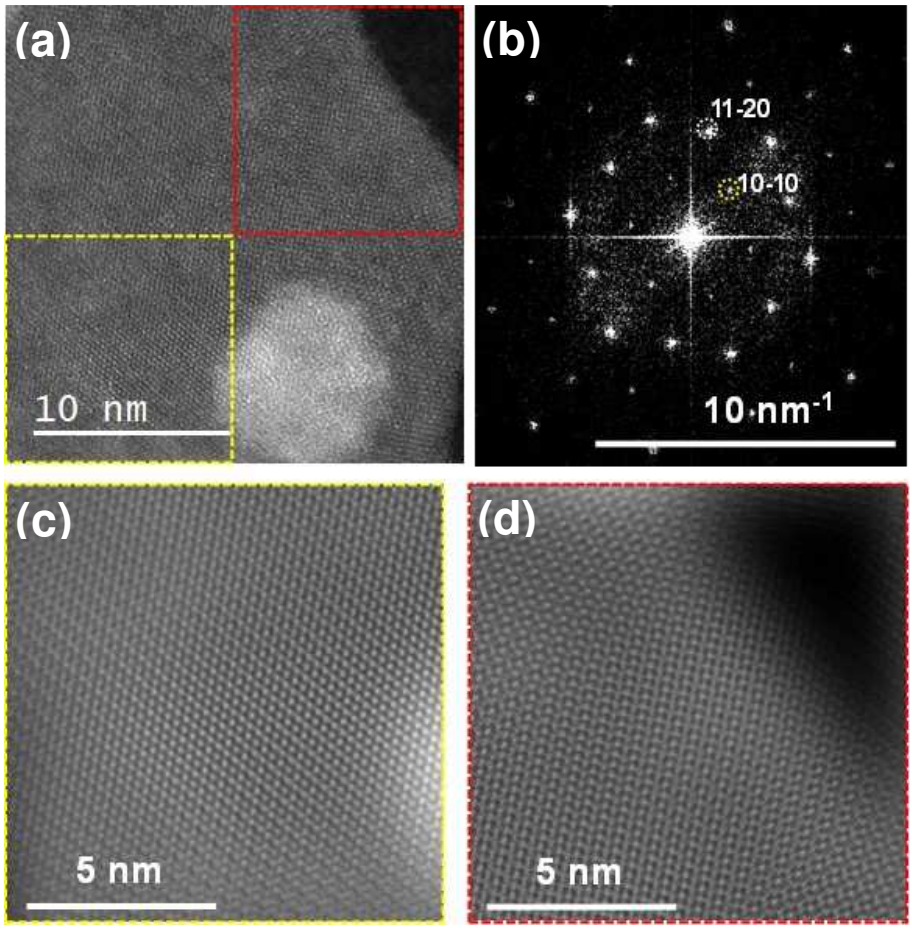

Fig. 6. (a) HAADF-STEM image of a nanoparticle present in the powder prepared at 41 °C.min^{-1}; (b) Calculated FFT indexed as a single hexagonal crystal in [0001] zone axis with parameter a = 5.85 Å ; (c) and (d) filtered images of down left part (c) and up right part (d) of the crystal showing different local atomic pattern.

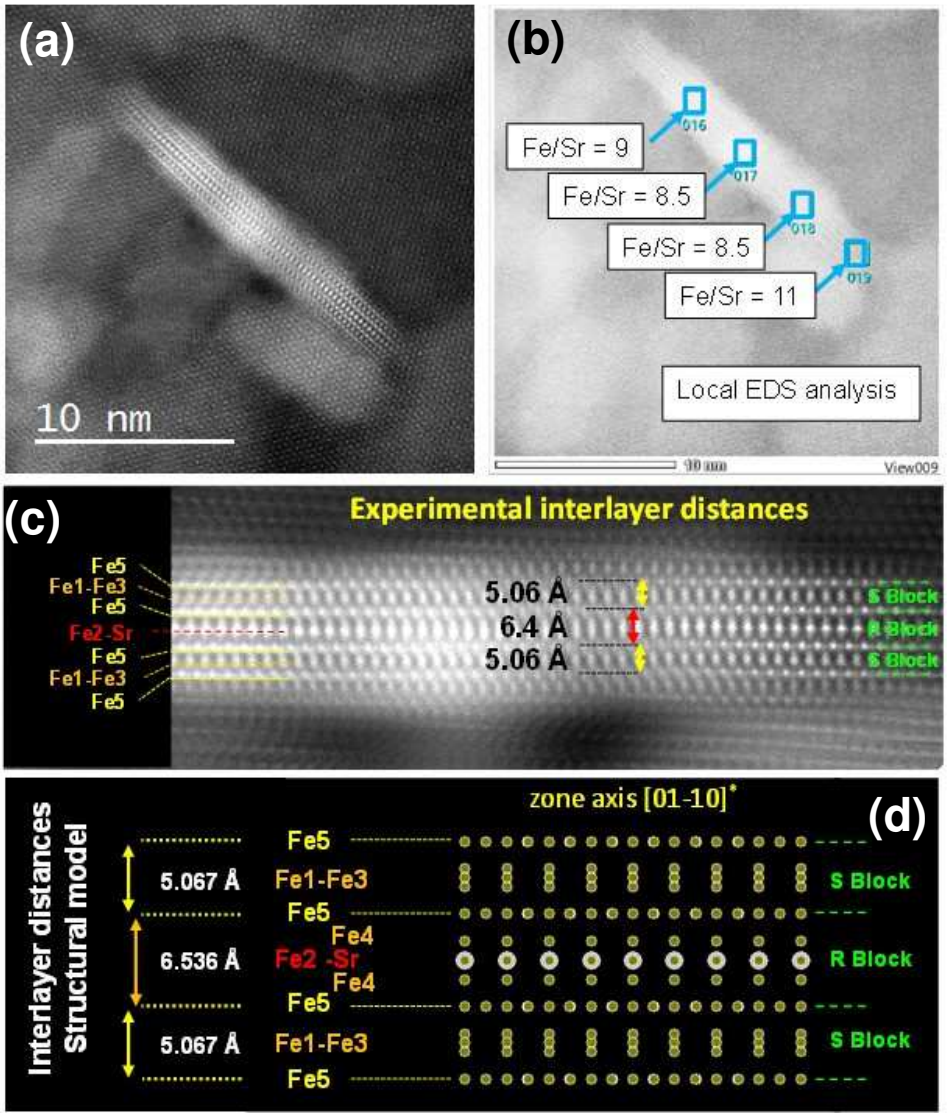

Fig. 7. (a) HAADF-STEM image of an 18 nm large hexaferrite-like platelet viewed edgewise; (b) EDS analysis along the central part of the platelet showing a Sr content higher than the strontium hexaferrite stoichiometry; (c) Fourier filtered image of the platelet with experimental interlayer distances similar to the expected ones ; (d) Metal atom columns of the $SrFe_{12}O_{19}$ hexaferrite structure in the $(01\bar{1}0)$ zone axis, Sr atoms in light grey and Fe atoms in brown.

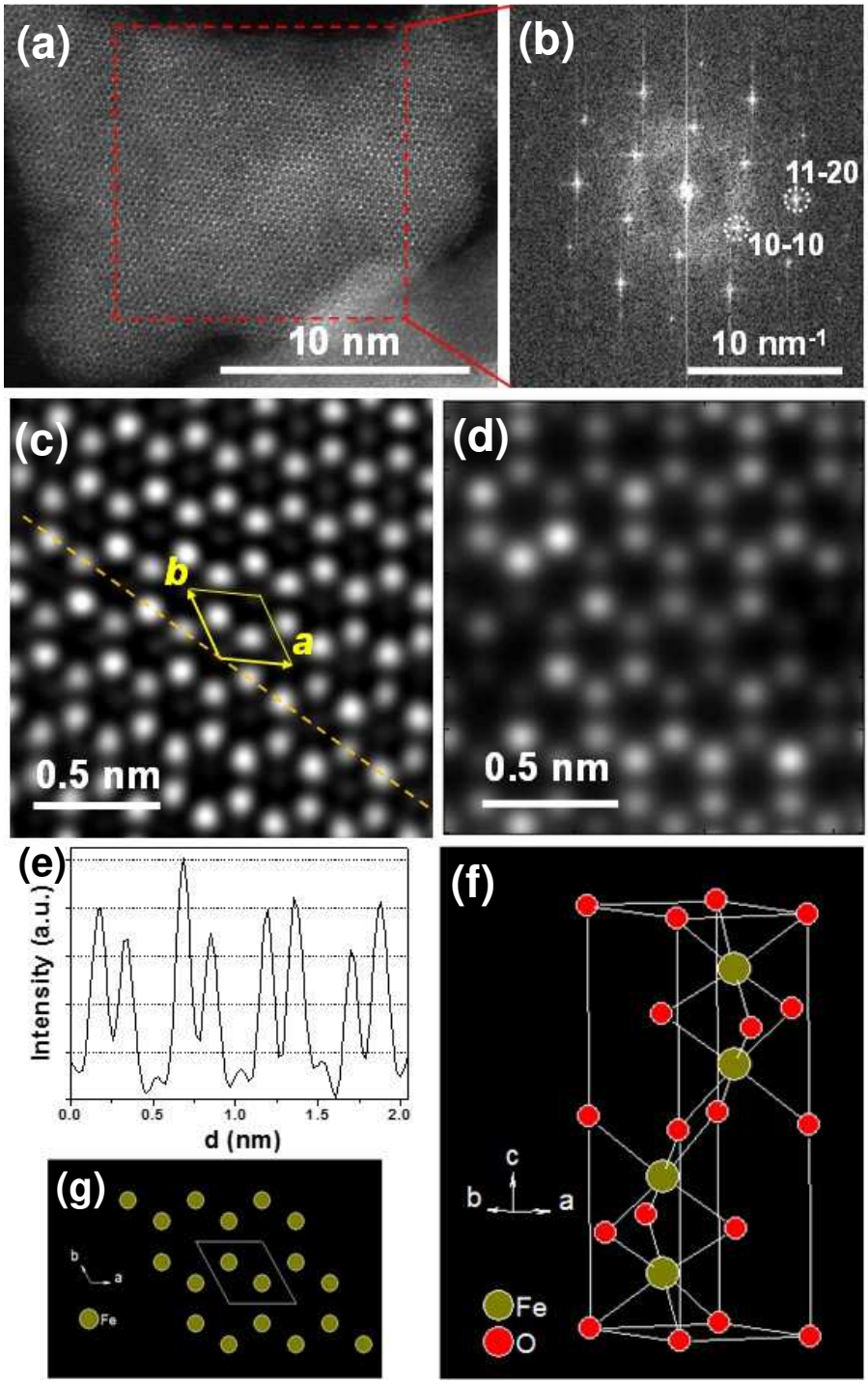

Fig. 8. (a) HAADF-STEM image of a nanoparticle present in the powder prepared at 49 °C.min^{-1}; (b) Calculated FFT of the central part of the HAADF image indexed as a hexagonal crystal in [0001] zone axis with parameter a = 2.9 Å; (c) Zoom on the Fourier filtered HAADF image; (d) HAADF-STEM image simulation of a 8 nm thick defect free ferrihydrite; (e) Intensity profile along the $[1\bar{1}00]^*$ direction (dashed line on filtered image) ; (f) Unit cell of the defect-free ferrihydrite ; (g) Projection of the Fe columns in the (0001) plane.

3.3. Discussion

Pure M-$SrFe_{12}O_{19}$ hexaferrite powders were prepared by microwave assisted hydrothermal method with an optimized HR of about 25 °C.min^{-1}. With higher HRs the powders were identified by XRD as mixtures of ferrihydrite and hexaferrite phases with M-type strontium hexaferrite lines that progressively vanished with increasing HR. The very small particle size and the cation disorder make complex the XRD pattern analysis. Electron microscopy in the HAADF-STEM mode coupled with local EDS analysis was used to have a deeper review of the ultra-small particles prepared with high heating rates. This study revealed a much more complex situation than simple mixtures of these two phases. Most of the particles contained strontium as inferred from EDS measurements discarding that pure ferrihydrite could be the major phase. Well-crystallized hexaferrite, and defect free ferrihydrite were found in these powders but were in minority. The most frequently observed particles exhibited a hexagonal structure with parameter *a* very close to M-$SrFe_{12}O_{19}$ type but with strongly disordered cation sites occupancy on the Fe and Sr sites like the example of Figure 6. Platelets consisting in a well-crystallized M-type strontium hexaferrite core but extending over less than a unit cell along c-direction and with surface disorder, as was inferred from the edgewise platelet analysis, can be the main component of the powders. Finally, well crystallized particles with Sr content higher than the hexaferrite stoichiometry exhibiting a distorted hexagonal structure were also identified.

The low saturation magnetization of these samples can be explained by the disorder on metal atom occupancy in ultra-small hexaferrite-like particles and by the presence of ferrihydrite-like particles. Makovec *et al.* suggested in a previous study that strongly disordered particles with M-type strontium hexaferrite-like structure may be paramagnetic or antiferromagnetic at room temperature because of disordered cation occupancy [19]. After annealing the crystallization of the small hexaferrite particles and the reaction between ferrihydrite and Sr-rich particles gave mainly the M-$SrFe_{12}O_{19}$ phase, increasing significantly the saturation magnetization and coercivity.

The high H_C values obtained after annealing are mainly due to the small particle size in the microwave hydrothermal step. The particle mean size depends on the nucleation rate. By increasing HR in the microwave process the number of seeds was increased and the particle mean size was reduced. In case of edgewise platelets it has been possible to identify the SRS stacking along the *c* axis showing that the metal atom stacking is symmetrical starting from a central layer

that contains the Sr atoms. This situation is different from what observed B. Belec *et al.* in a previous study on $BaFe_{12}O_{19}$-like ultrathin particles [21]. The platelets in that case were identified mainly as SRSRS stacking i.e. symmetrical from a S block. The SRSRSRS stacking was also observed but as minor product [21]. It suggests that the nucleation step of the ultrathin platelets depends on the composition of the starting mixture. In the present study the nuclation involved clusters containing Sr ions in agreement with an excess of strontium in the starting mixture.

4. Conclusion

The microwave-assisted hydrothermal process is a versatile method to synthesize in short reaction times pure M-type strontium hexaferrite powders or mixtures of strontium hexaferrite and ferrihydrite-like particles depending on the heating rate. Pure M-$SrFe_{12}O_{19}$ particles with platelet shape and mean diameter in the micrometer range were prepared by optimizing the heating rate at around 25 °C.min^{-1}. These particles exhibited a saturation magnetization close to the bulk after annealing at 1000 °C and a high coercivity. By increasing the microwave heating rate in the range 40-50 °C.min^{-1} the particle size and their aspect ratio were decreased. HAADF-STEM imaging and EDS analysis of the ultra-small particles showed well-crystallized nanoparticles with local variations in Sr-content. Atomic scale resolution analysis showed that, besides hexaferrite and ferrihydrite, particles crystallizing with a hexaferrite core extending over less than a unit cell and with surface disorder were the major population. The multilayer stacking SRS observed in several edgewise particles suggests that the nucleation step of these particles involved cluster containing Sr atoms. After annealing the powders exhibited a higher coercivity thanks to smaller particle size and a reasonable saturation magnetization thanks to a limited amount of hematite.

Supporting Information

Supplementary data associated with this article can be found in the online version

Acknowledgements

The authors would like to thank L. Datas and T. Hungria (Plateforme Castaing, Toulouse, France) for the HAADF-STEM experiments. C. M. and G. V. gratefully acknowledge the European Associated Laboratory (LEA)-TALEM2.

References

[1] O. Gutfleisch, M. A. Willard, E. Brück, C. H.Chen, S. G. Sankar, J. P. Liu, *Adv. Mater.* **23** (2011) 821.

[2] R.C. Pullar, Prog. *Mater Sci.* 57 (2012) 1191.

[3] A. Ataie, S. Heshmati-Manesh, *J. Eur. Ceram. Soc.* 21 (2001) 1951.

[4] M. Drofenik, M. Kristl, A. Znidargic, D. Hanmel, D. Lisjak, *J. Am. Ceram. Soc.* 90 (2007) 2057.

[5] M. Jean, V. Nachbaur, J. Bran, J. –M. Le Breton, *J. Alloys Compds.* 496 (2010) 306.

[6] D. Primc, M. Drofenik, D. Makovec, *Eur. J. Inorg. Chem.* (2011) 3802.

[7] A. Xia, C. Zuo, L. Chen, C. Jin, Y. Lv, *J. Magn. Magn. Mater.* 332 (2013) 186.

[8] T. Yamauchi, Y. Tsukahara, T. Sakata, H. Mori, T. Chikata, S. Katoh, Y. Wada, *J. Magn. Magn. Mater.* 321 (2009) 8.

[9] X. Meng, S. Xu, J. Zhou, Q. Tang, *Ceram. Intern.* 42 (2016) 6025.

[10] C.-Y. Xu, L.-S. Fu, X. Cai, X.-Y. Sun, L. Zhen, *Ceram. Intern.* 40 (2014) 8593.

[11] L. Wu, B. Shen, S. Sun, *Nanoscale* 7 (2015) 16165.

[12] T. Zhang, X. Peng, J. Li,Y. Yang, J. Xu, P. Wang, D. Jin, H. Jin, B. Hong, X. Wang, H. Ge, *J. Magn. Magn. Mater* 412 (2016) 102.

[13] D. Lisjak, S. Ovtar, *Langmuir* 27 (2011) 14014.

[14] D. Primc, D. Makovec, D. Lisjak, M. Drofenik, *Nanotechnology* 20 (2009) 315605.

[15] S. E. Kushnir, A. I. Gavrilov, P. E. Kazin, A. V. Grigorieva, Y. D. Tretyakovab, M. Jansen, *J. Mater. Chem.* 22 (2012) 18893.

[16] A. Mertelj, D. Lisjak, M. Drofenik, M. Čopič, *Nature* 504 (2013) 237.

[17] M. Saura-Múzquiz, C. Granados-Miralles, M. Stingaciu, E. Drath Bøjesen, Q. Li, J. Song, M. Dong, E. Eikelanda, M. Christensen, *Nanoscale* 8 (2016) 2857.

[18] D. Primc, D. Makovec, *Nanoscale* 7 (2015) 2688.

[19] D. Makovec, D. Primc, S. Sturm, A. Kodre, D. Hanzel, M. Drofenik, *J. Solid State Chem.* 196 (2012) 63.

[20] C. Granados-Miralles, M. Saura-Múzquiz, E. D. Bøjesen, K. M. Ø. Jensen, H. L. Andersen, M. Christensen, *J. Mater. Chem. C* 4 (2016) 10903.

[21] B. Belec, G. Dražić, S. Gyergyek, B. Podmiljšak, T. Goršak, M. Komelj, J. Nogués, D. Makovec, *Nanoscale* 9 (2017) 17551.

[22] H.M. Rietveld, *J. Appl. Crystallogr.* 2 (1969) 65.

[23] J.R. Carvajal, Computer Program FullProf and WinPLOTR, Laboratoire Léon Brillouin CEA-CNRS, Grenoble 1998.

[24] C. Kock. Determination of core structure periodicity and point defect density along dislocations", Doctoral Thesis, Arizona State University, 2002.

[25] T. S. Berquó, S. K. Banerjee, R. G. Ford, R. L. Penn, T. Pichler, *J. Geophys. Res.* 112 (2007) B02102.

[26] V. A. Drits, B. A. Sakharov, A. L. Salyn, A. Manceau, *Clay Minerals* 28 (1993) 185.

[27] E. Jansen, A. Kyek, W. Schafer, U. Schwertmann, *Applied Physics* A 74 (2002) S1004.

[28] D. E. Janney, J. M. Cowley, P. R. Buseck, *Am. Mineral.* 86 (2001) 327.

[29] A. Manceau, *Am. Mineral.* 96 (2011) 521.

[30] A. Manceau, S. Skanthakumar, L. Soderholm, *Am. Mineral.* 99 (2014) 102.

[31] H. Kojima, Fundamental properties of hexagonal ferrites with magnetoplumbite structure, in Ferromagnetic Material, Vol 3 (ed E.P. Wohlfarth), North Holland, Amsterdam, The Netherlands, 1982.

[32] B. Grindi, Z. Beji, G. Viau, A. BenAli, *J. Magn. Magn. Mater.* 449 (2018) 119.

[33] U. Schwertmann, J. Friedl, H. Stanjek, *J. Colloid Interface Sci.* 209 (1999) 215.

[34] Y. Cudennec, A. Lecerf, *J. Solid State Chem.* 179 (2006) 716.

[35] ICDD file 01-080-1197.

SUPPORTING INFORMATION

M-$SrFe_{12}O_{19}$ and Ferrihydrite-like Ultrathin Nanoplatelets as Building Blocks for Permanent Magnets: HAADF-STEM Study and Magnetic Properties

Bilel Grindi, Amor BenAli, Cesar Magen, Guillaume Viau

List of supplementary figures

Figures S1. (a) Unit cell of $SrFe_{12}O_{19}$, hexagonal system, $P6_3/mmc$ space group (no. 194), Unit cell dimensions a = 5.9320 Å, c = 23.2060 Å; (b) projection of the Fe and Sr columns in the (0001) plane ; (c) metal atom labels; (d) projections of the labelled metal atoms.

Figure S2. Crystallographic structure of defect free ferrihydrite according to Jansen et al. [Reference E. Jansen, A. Kyek, W. Schafer, U. Schwertmann, *Appl. Phys.* A, **2002**, *74*, S1004-S1006 ; COD file 9012762]. (a) Unit cell of defect free ferrihydrite (f-phase): trigonal system, $P\text{-}3_1c$ space group (no. 163), unit cell dimensions a = 2.9550 Å, c = 9.3700 Å; (b) projection of the Fe atoms in the (0001) plane (Fe occupancy is 0.39).

Figure S3. Crystallographic structure of defective ferrihydrite according to according to Jansen et al. [Reference E. Jansen, A. Kyek, W. Schafer, U. Schwertmann, *Appl. Phys.* A, **2002**, *74*, S1004-S1006 ; COD file 9012761]. (a) Unit cell of defective ferrihydrite (d-phase): trigonal system, P3 space group (no. 143), unit cell dimensions a = 2.9550 Å, c = 9.3700 Å ; (b) Projection of the Fe atoms in the (0001) plane (Fe occupancy is 0.24).

Figure S4. Crystallographic structure of hematite. (a) Unit cell of hematite: trigonal system, R-3c space group (no. 167), unit cell dimensions a = 5.431 Å, α = 55.23 °; (b) Projection of the Fe atoms along the [111] axis.

Figure S5. XRD pattern of powders obtained after annealed at 1000 °C for one hour of sample synthesis with different heating rate (a) 12°C/min, (b) 27°C/min, (c) 35°C/min, (d) 41°C/min and (e) 49°C/min. Inset: zoom of the pattern in the 2θ range 37-41° revealing the presence of hematite (asterisk denotes the (104) reflexion of hematite).

Figure S6. SEM images of particles obtained with different heating rate annealed at 1000 °C, (a) 12°C/min, (b) 27°C/min, (c) 41°C/min and (d) 49°C/min.

Figure S7. HAADF-STEM images and EDS analyses of particles prepared with a heating rate of 41 °C.min^{-1}. The Fe/Sr molar ratio measured on large areas is close to 12..

Figure S8. HAADF-STEM image and local EDS analysis of a platelet identified as $SrFe_{12}O_{19}$ hexaferrite in (0001) zone axis on the Fourier filtered image: (a) STEM-HAADF image and local Fe/Sr ratio measured by EDS ; (b) Fourier filtered images of the analyzed area showing the typical pattern of hexaferrite $SrFe_{12}O_{19}$ in (0001) zone axis.

Figure S9. (a) HAADF-STEM image of a 2.7-3 nm thick platelet viewed edge wise ; (b) Fourier filtered image of the red square area showing an atomic pattern similar to a hexaferrite core on [10-10]* zone axis. Like in the example given in Figure 7 of the main text, the crystallized part of the platelet consists in a S-R-S blocks stacking.

Figure S10. (a) HAADF-STEM image of a defect free ferrihydrite platelet viewed edgewise ; (b) Fourier filtered image of the yellow square ; (c) zoom on the filtered image (the image has been tilted for clarity); (d) Projection of the cationic columns for the defect free ferrihydrite structure in (1-210) zone axis showing a strong analogy with the experimental pattern.

Figure S11. (a) HAADF-STEM image and local EDS analysis of a platelet that does not contain Sr ; (b) Calculated Fourier transform of the white square indexed as a hexagonal structure in (0001) zone axis and with parameter a = 2.9 Å; (c) Zoom on the Fourier filtered image of the white square ; (d) HAADF-STEM image simulation of a 8 nm thick defective ferrihydrite particle in (0001) zone axis; (e) Unit cell of defective ferrihydrite; (f) Projection of the cationic columns of defective ferrihydrite in the (0001) zone axis; (g) Unit cell of hematite; (h) Projection of the cationic columns of hematite in the (111) zone axis.

Figure S12. (a) HAADF-STEM image of Sr-rich nanoparticle (Fe/Sr ratio given by EDS analysis = 7) ; (b) Calculated FFT of the zone framed by the blue square; (c) Fourier filtered image of the blue square zone and intensity profiles along the lines L1, L2 and L3 ; (d) Projection of the orthorhombic cell of the (e) Typical Fourier filtered image of a M-$SrFe_{12}O_{19}$ hexaferrite particles with the projection of the hexagonal cell, as a matter of comparison.

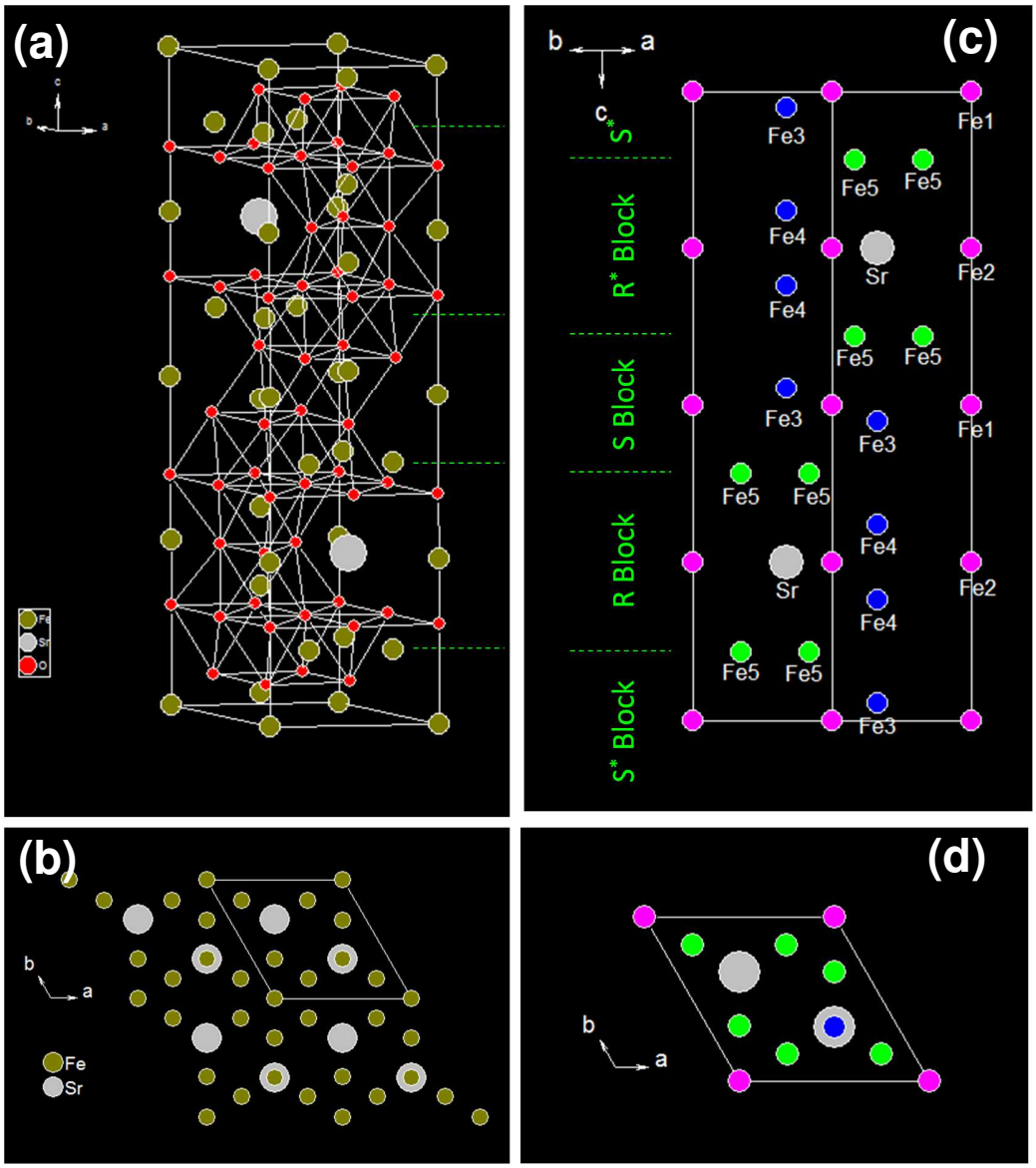

Figures S1. (a) Unit cell of $SrFe_{12}O_{19}$, hexagonal system, $P6_3/mmc$ space group (no. 194), Unit cell dimensions a = 5.9320 Å, c = 23.2060 Å; (b) projection of the Fe and Sr columns in the (0001) plane ; (c) metal atom labels; (d) projections of the labelled metal atoms.

Atom label	**Wyckoff position**
Fe1	2*a*
Sr1	2*d*
Fe2	2*b*
Fe3	4*f*
Fe4	4*f*
Fe5	12*k*

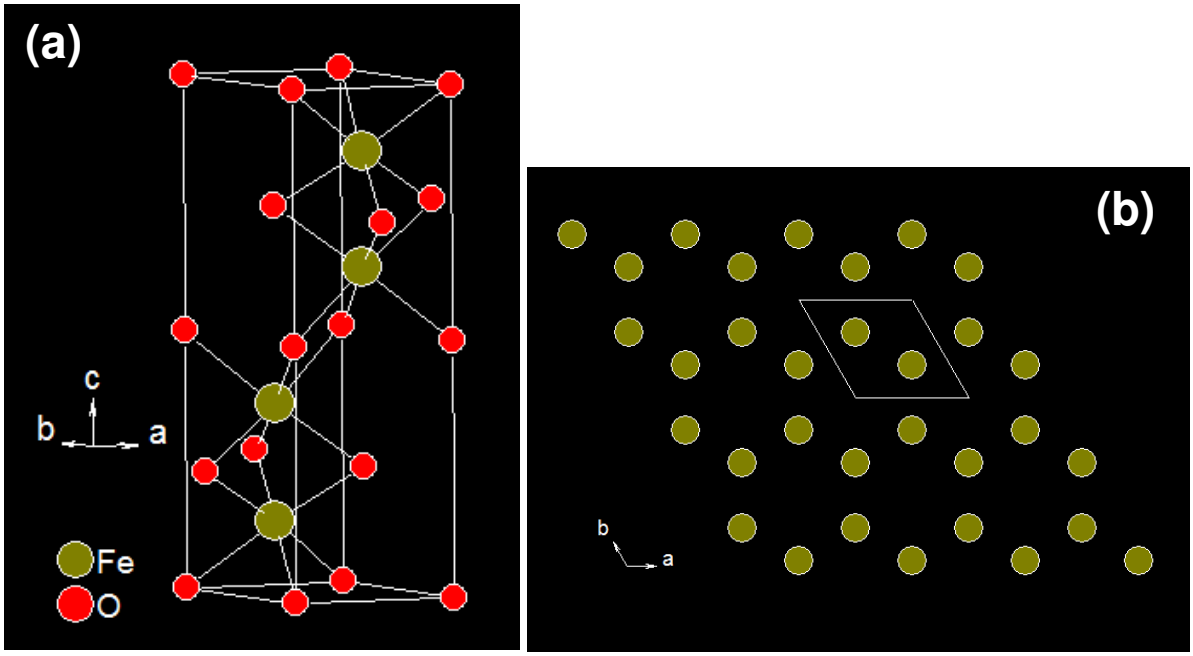

Figures S2. Crystallographic structure of defect free ferrihydrite according to Jansen et al. [Reference E. Jansen, A. Kyek, W. Schafer, U. Schwertmann, *Appl. Phys.* A, **2002**, *74*, S1004-S1006 ; COD file 9012762]. (a) Unit cell of defect free ferrihydrite (f-phase): trigonal system, P-3_1c space group (no. 163), unit cell dimensions a = 2.9550 Å, c = 9.3700 Å; (b) projection of the Fe atoms in the (0001) plane (Fe occupancy is 0.39).

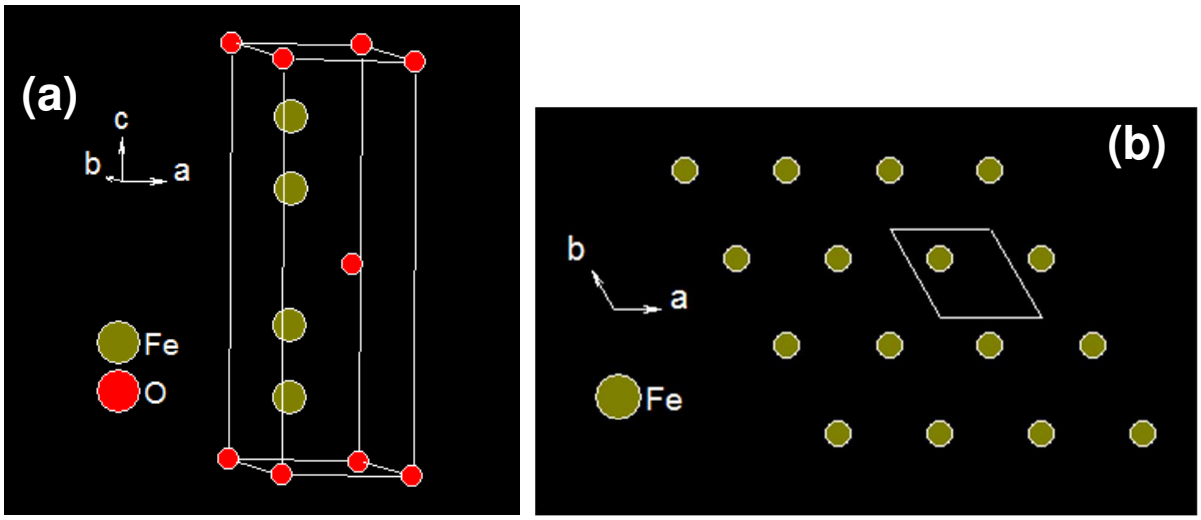

Figures S3. Crystallographic structure of defective ferrihydrite according to according to Jansen et al. [Reference E. Jansen, A. Kyek, W. Schafer, U. Schwertmann, *Appl. Phys.* A, **2002**, *74*, S1004-S1006 ; COD file 9012761]. (a) Unit cell of defective ferrihydrite (d-phase): trigonal system, P3 space group (no. 143), unit cell dimensions a = 2.9550 Å, c = 9.3700 Å ; (b) Projection of the Fe atoms in the (0001) plane (Fe occupancy is 0.24).

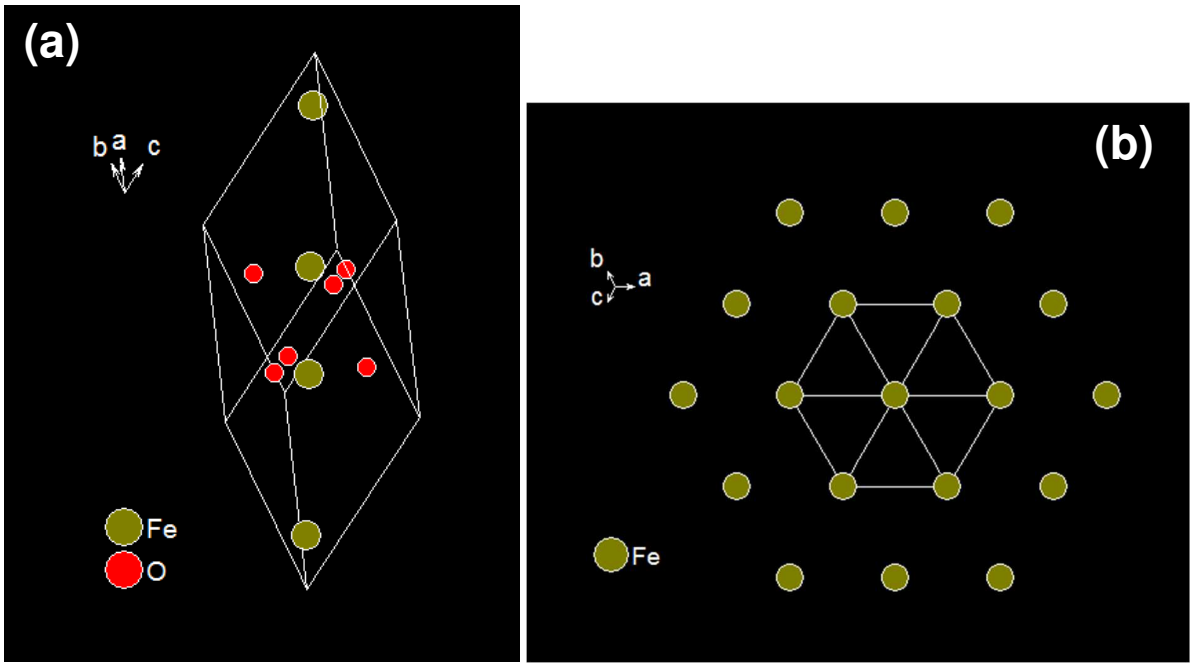

Figures S4. (a) Unit cell of hematite: trigonal system, R-3c space group (no. 167), unit cell dimensions a = 5.431 Å, α = 55.23 °; (b) Projection of the Fe atoms along the [111] axis.

Note that the projection of the Fe columns along the [111] axis is similar to the projection of the Fe columns of the defective ferrihydrite along the [0001] axis, see figure S3. The smallest distance between the Fe columns is 2.9 Å in both cases.

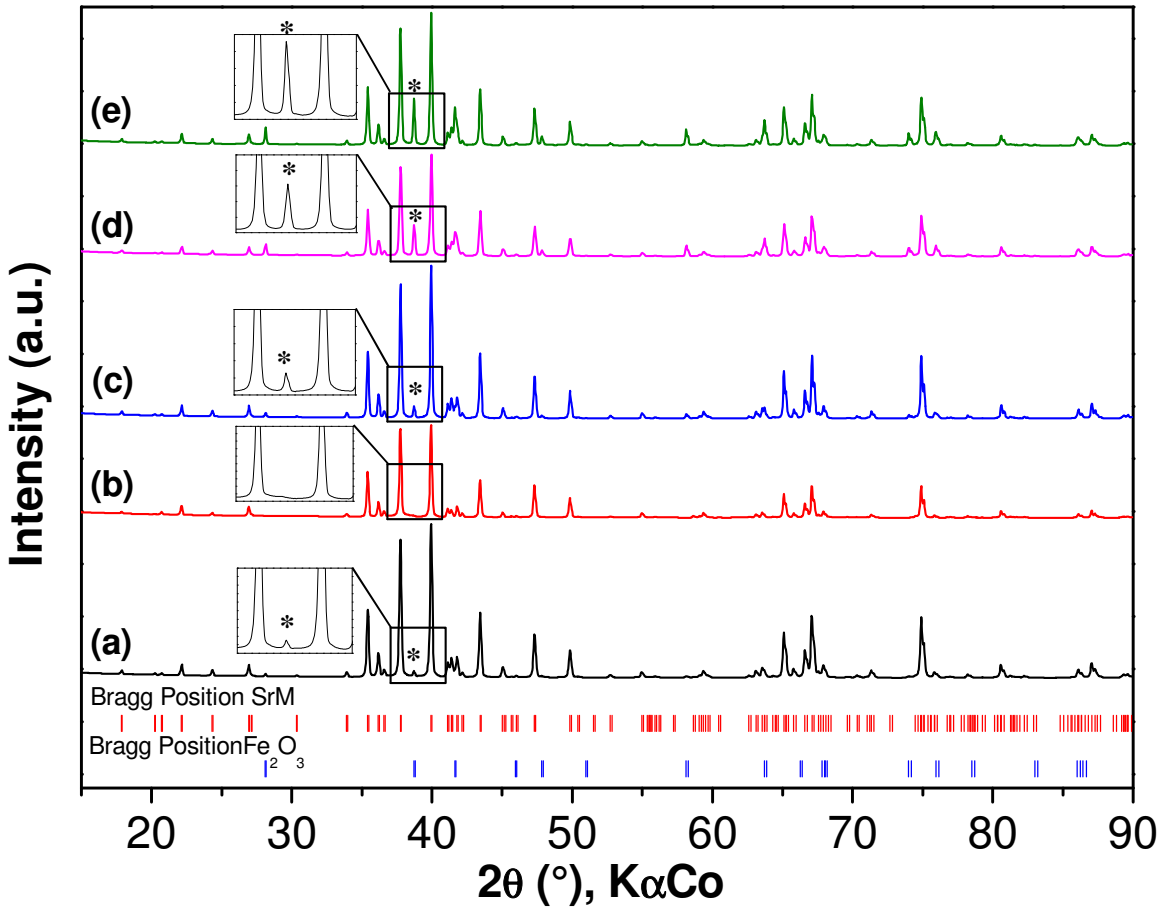

Figure S5. XRD pattern of powders obtained after annealed at 1000 °C for one hour of sample synthesis with different heating rate (a) 12°C/min, (b) 27°C/min, (c) 35°C/min, (d) 41°C/min and (e) 49°C/min. Inset: zoom of the pattern in the 2θ range 37-41° revealing the presence of hematite (asterisk denotes the (104) reflexion of hematite).

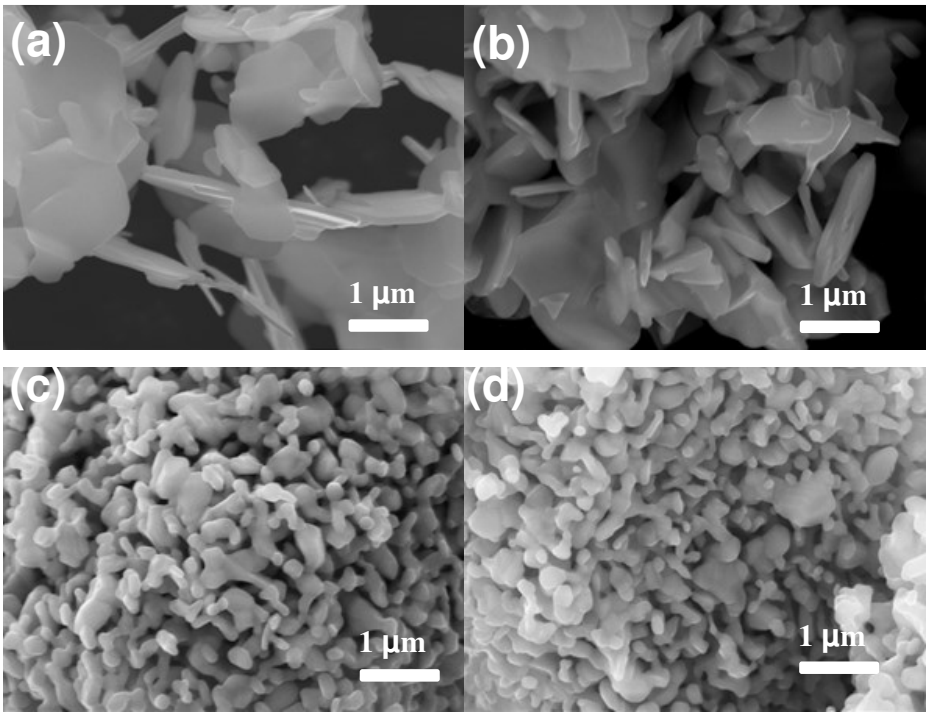

Figure S6. SEM images of particles obtained with different heating rate annealed at 1000 °C, (a) 12°C/min, (b) 27°C/min, (c) 41°C/min and (d) 49°C/min.

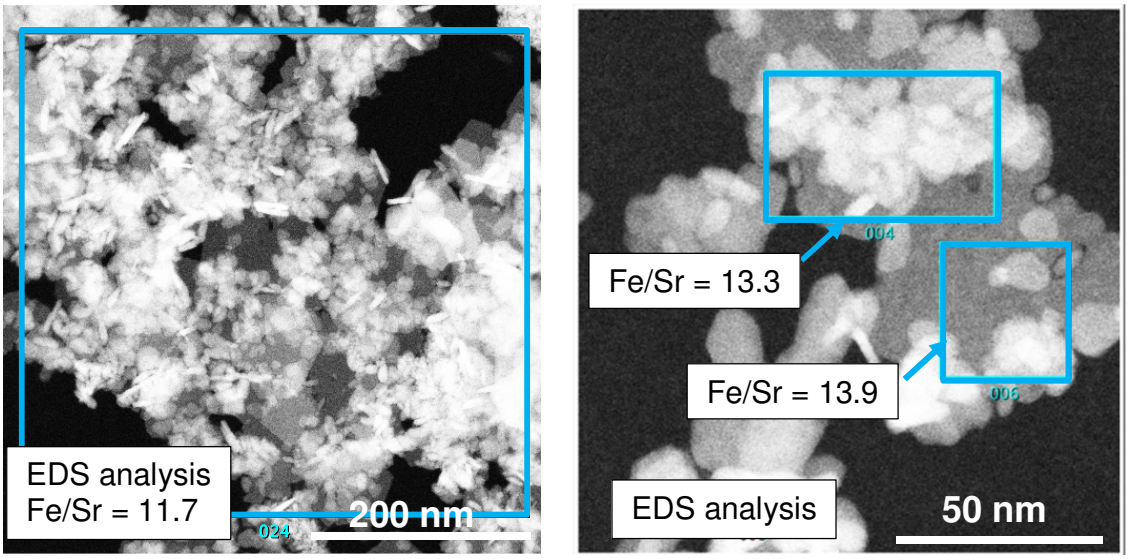

Figure S7. HAADF-STEM images and EDS analyses of particles prepared with a heating rate of 41 °C.min^{-1}. The Fe/Sr molar ratio measured on large areas is close to 12.

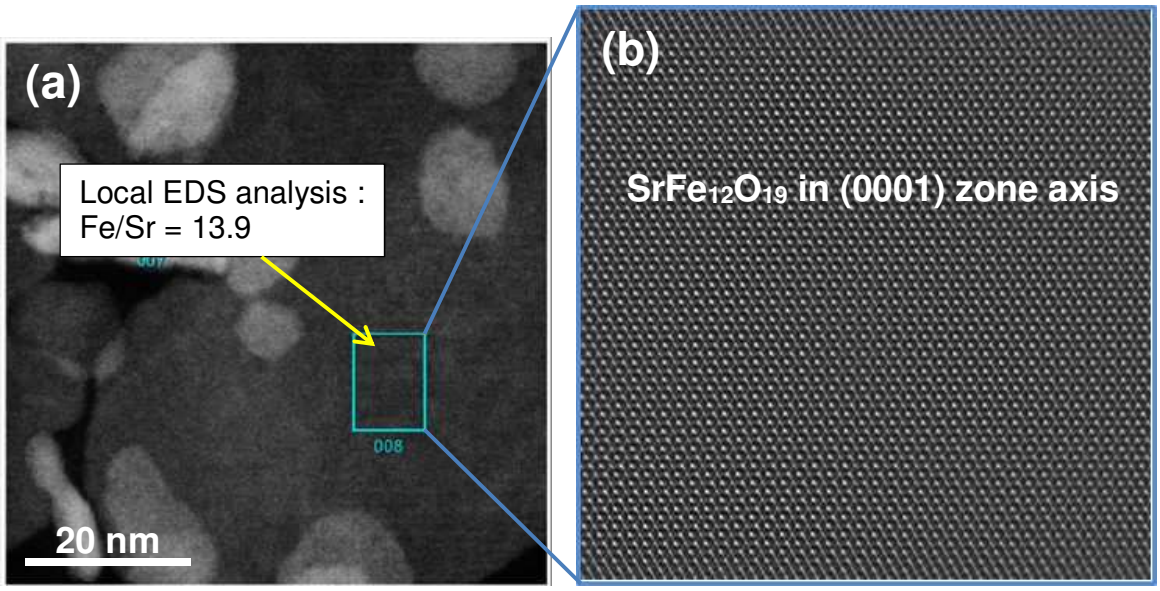

Figure S8. HAADF-STEM image and local EDS analysis of a platelet identified as $SrFe_{12}O_{19}$ hexaferrite in (0001) zone axis on the Fourier filtered image: (a) STEM-HAADF image and local Fe/Sr ratio measured by EDS ; (b) Fourier filtered images of the analyzed area showing the typical pattern of hexaferrite $SrFe_{12}O_{19}$ in (0001) zone axis.

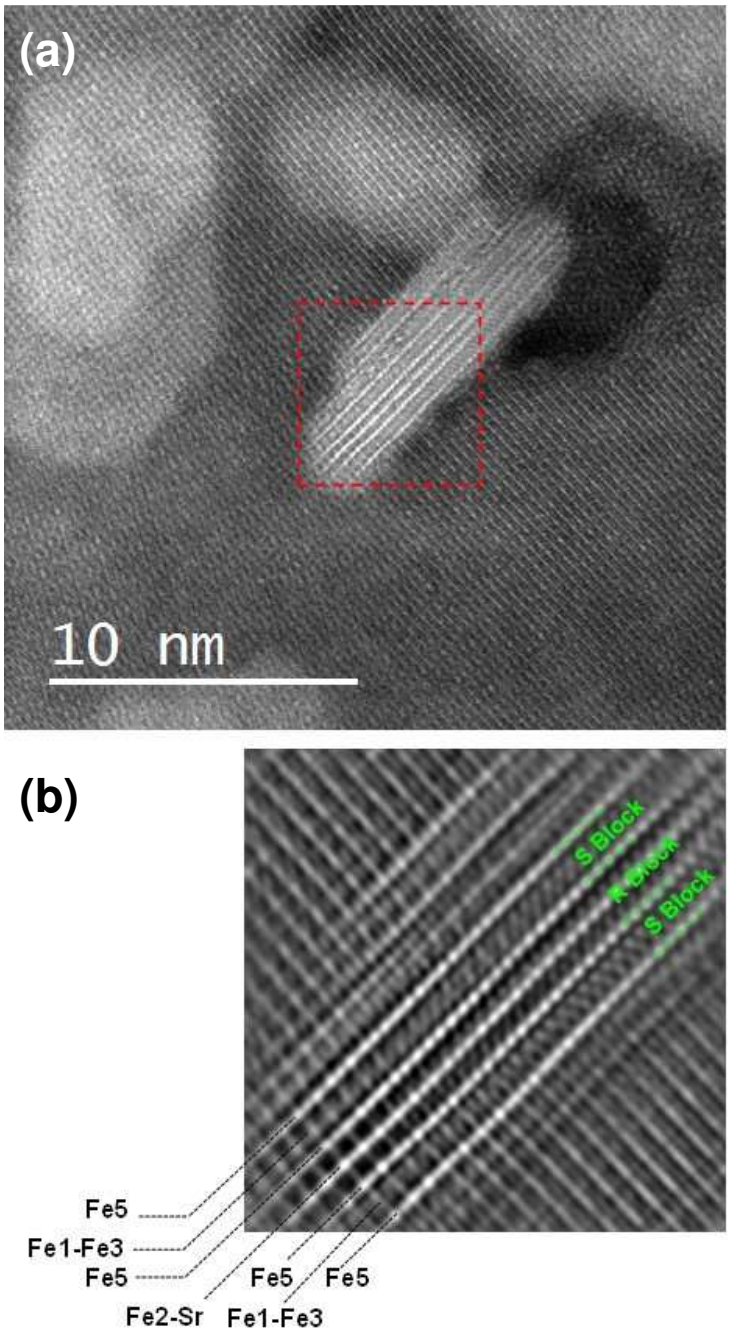

Figure S9. (a) HAADF-STEM image of a 2.7-3 nm thick platelet viewed edge wise ; (b) Fourier filtered image of the red square area showing an atomic pattern similar to a hexaferrite core on [10-10]* zone axis. Like in the example given in Figure 7 of the main text, the crystallized part of the platelet consists in a S-R-S blocks stacking.

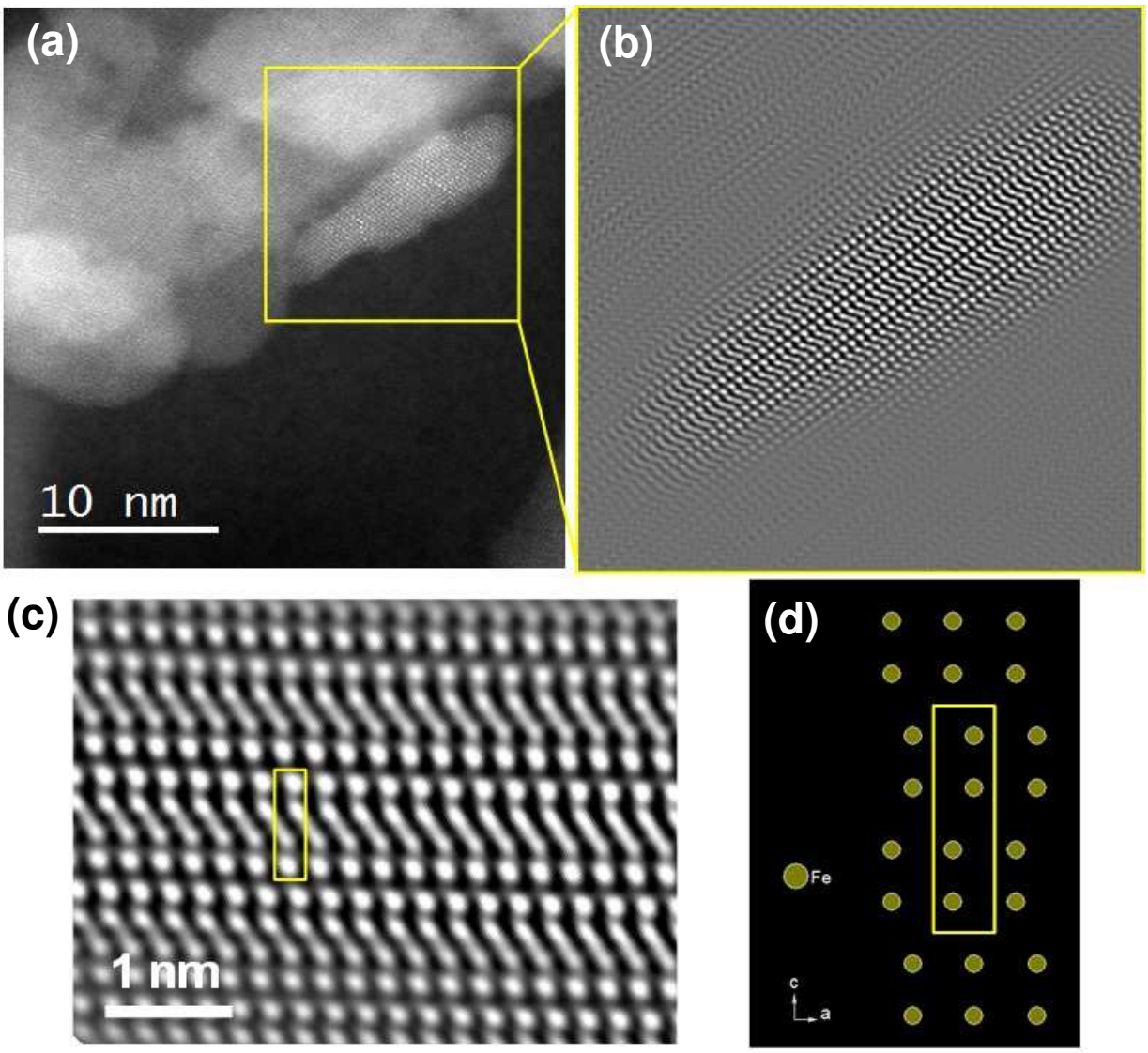

Figure S10. (a) HAADF-STEM image of a defect free ferrihydrite platelet viewed edgewise ; (b) Fourier filtered image of the yellow square ; (c) zoom on the filtered image (the image has been tilted for clarity); (d) Projection of the cationic columns for the defect free ferrihydrite structure in (1-210) zone axis showing a strong analogy with the experimental pattern.

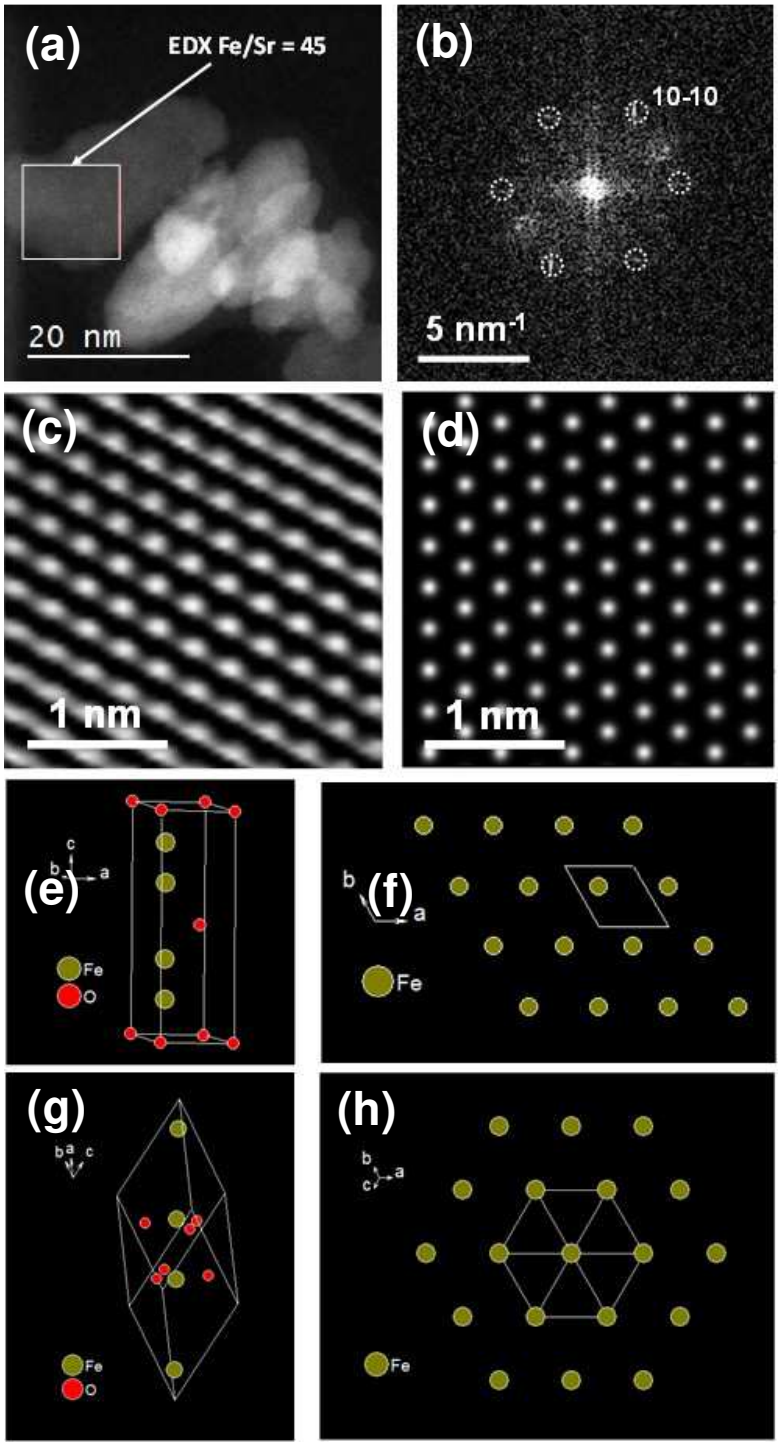

Figure S11. (a) HAADF-STEM image and local EDS analysis of a platelet that does not contain Sr ; (b) Calculated Fourier transform of the white square indexed as a hexagonal structure in (0001) zone axis and with parameter a = 2.9 Å; (c) Zoom on the Fourier filtered image of the white square ; (d) HAADF-STEM image simulation of a 8 nm thick defective ferrihydrite particle in (0001) zone axis; (e) Unit cell of defective ferrihydrite; (f) Projection of the cationic columns of defective ferrihydrite in the (0001) zone axis; (g) Unit cell of hematite; (h) Projection of the cationic columns of hematite in the (111) zone axis.

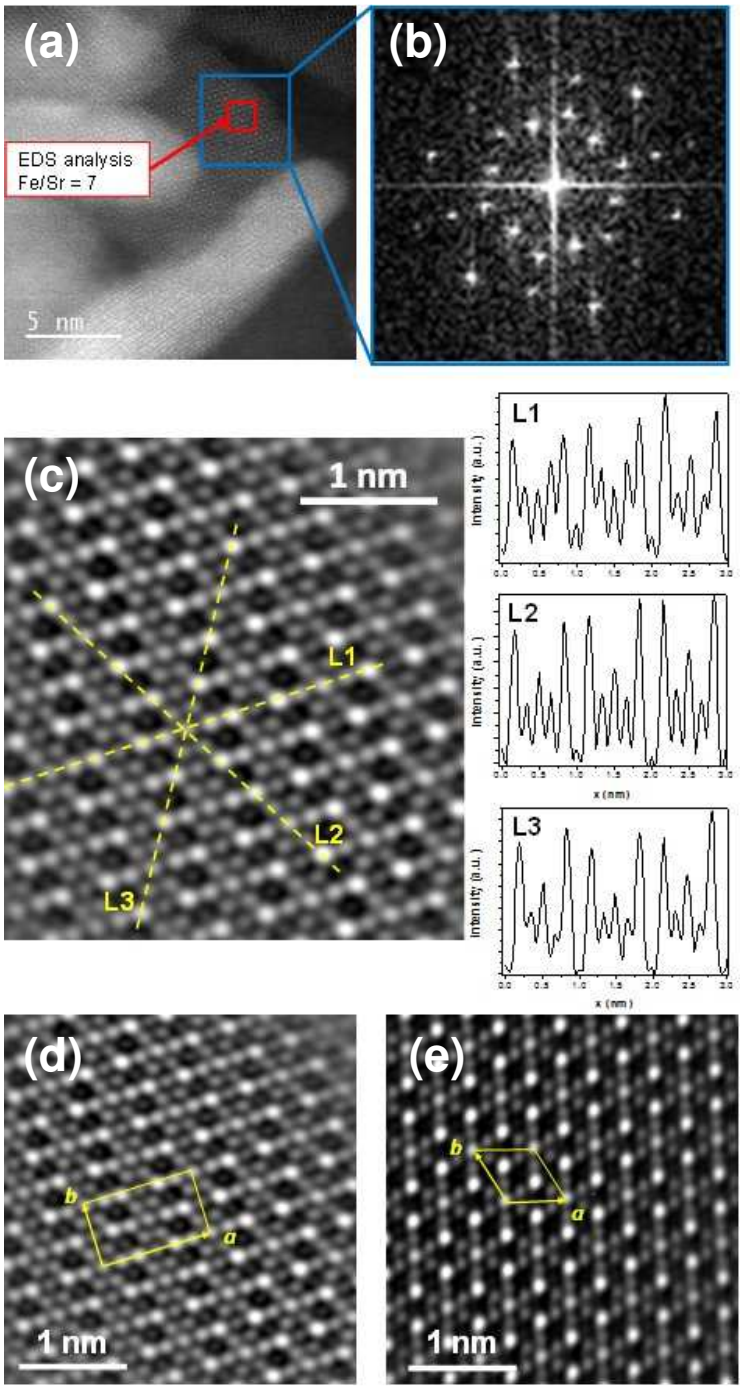

Figure S12. (a) HAADF-STEM image of Sr-rich nanoparticle (Fe/Sr ratio given by EDS analysis = 7) ; (b) Calculated FFT of the zone framed by the blue square; (c) Fourier filtered image of the blue square zone and intensity profiles along the lines L1, L2 and L3 ; (d) Projection of the orthorhombic cell of the (e) Typical Fourier filtered image of a M-$SrFe_{12}O_{19}$ hexaferrite particles with the projection of the hexagonal cell, as a matter of comparison.

Comment on figure S12:

The calculated FFT of figure S12b presents some similarities with the FFT pattern of a pure hexaferrite particle (see Fig. 5b of the article) but the spots do not form a regular hexagon showing an orthorhombic distortion with respect to the pure hexaferrite structure.

The comparison of the Fourier filtered HAADF image of the Sr-rich particle and of a typical hexaferrite particle shows that the atomic pattern are different (Fig. S12d-e). The scattering intensity along three pseudo $[10\bar{1}0]$* directions (L1, L2 and L3) are plotted on Figure S12c. The intensity profile along L1 is very different from the profile of an hexaferrite particle (see for example Fig. 5 of the article). In contrast the intensity profiles along L2 and L3 were similar to the profile measured on the hexaferrite HAADF images with a periodicity over five atomic columns (Fig. S12c). This result confirm the orthorhombic distortion.